European Polymer Journal 176 (2022) 111398

Contents lists available at ScienceDirect

European Polymer Journal

journal homepage: www.elsevier.com/locate/europolj

The effects of silica aerogel on the rheological behaviour and polymer matrix structure of Rigid Polyurethane foams

Paula Cimavilla-Román [a,*], Saul Perez-Tamarit [a], Anja Vananroye [b], Paula Moldenaers [b], Miguel Ángel Rodriguez-Pérez [a,c]

[a] Cellular Materials Laboratory (CellMat), Condensed Matter Physics Department, University of Valladolid, Spain
[b] Department of Chemical Engineering, KU Leuven, Leuven, 3001, Belgium
[c] BioEcoUva. Research Institute on Bioeconomy, University of Valladolid, Spain

ARTICLE INFO

Keywords:
Polyurethane foam
Silica aerogel
Rheology
Reaction kinetics
X-ray tomography

ABSTRACT

The incorporation of silica aerogel particles into the isocyanate used to prepare Rigid Polyurethane composite foams drastically modifies its rheological behaviour. The isocyanate changes from being a Newtonian fluid of constant viscosity (0.3 Pa s at 25 °C) to a non-linear power-law material with complex viscosity decreasing from 10^4 to 10^1 Pa s with a slope −1 versus frequency. The change in response is caused by the formation of a percolated network of particles at contents above 2.5 wt% of aerogel. Moreover, the addition of aerogel significantly slows down the modulus-build up kinetics and vitrification of the matrix by approximately 4.5 min with every 1 wt% of aerogel added. For the foam with 3.0 wt% of aerogel, the combination of high viscosity at early reaction times coupled with the slow modulus build-up impedes the drainage which leads to a decrease in the fraction of material in the struts of the matrix.

1. Introduction

The production of polymer composite foams is a well-known strategy to enhance the properties of the starting material by introducing a small amount of a secondary phase [1]. Since their establishment, composite foams have been produced using a wide array of fillers as reinforcement (fibres, flakes, micro- and nanoparticles) and all types of polymer matrices (thermoplastic, thermosets, or elastomers). The use of fillers with different morphologies and properties is a way of tailoring the final composite foam performance and range of applications [2,3]. However, obtaining superior foams is also conditioned by the final foam structure, which is affected by the filler dispersion and the matrix-filler interactions during foaming.

Among composite foams, Rigid Polyurethane (RPU) composites are receiving increasing attention for their enhanced mechanical performance and improved thermal insulation. The former is achieved by introducing inorganic reinforcements, *i.e.,* glass fibres, while the latter relies on novel fillers with low thermal conductivity, *i.e.,* aerogels [3–6]. In the case of thermal insulation, PU-aerogel composite foams are promising materials due to the favourable aerogel properties of low density, low thermal conductivity and flame retardancy [7–11]. Recently, several studies have been published dealing with the structure-properties relationship in PU-aerogel composite foams. Zhao et al. prepared Polyisocyanurate rigid (PIR) foams with varying content of granular silica aerogel [8]. The foam with a high content of aerogel (8 wt%) showed a reduction of the thermal conductivity of 34.6%. However, the addition of aerogel particles does not always translate to a significant improvement of the original PU foam properties. In contrast, Kim et al. reported minimal thermal conductivity reductions when producing PU-silica aerogel foams [11]. This was attributed to the deterioration of the structure with increasing aerogel content. In terms of acoustic insulation notable enhancement was observed when producing Phenolic aerogel-flexible PU foams [10]. Improved sound absorption was attributed to a higher open porosity and reduced cell size caused by the phenolic aerogel incorporation. These discrepancies in the efficiency of aerogel particles are often attributed to either the presence of particle agglomerates or to a modification in the PU foaming reactions caused by the incorporation of the particles [12,13].

In a previous work, we evaluated the influence of different contents of powdered silica aerogel on the cellular structure generation and reaction kinetics of water-blown RPU foams [6]. The composite RPU-aerogel foams were produced using isocyanate-aerogel dispersions. It

* Corresponding author.
E-mail address: paulacimavilla@fmc.uva.es (P. Cimavilla-Román).

https://doi.org/10.1016/j.eurpolymj.2022.111398
Received 9 May 2022; Received in revised form 2 July 2022; Accepted 4 July 2022
Available online 6 July 2022

was observed that the final cellular structure of the composite foams was the result of a combination of increased nucleation as well as degeneration caused by the aerogel particles. Moreover, a dissimilar foaming process was observed with increasing aerogel content. It was observed that foams with low contents of aerogel particles (≤1 wt%) had a higher number of urethane cross-links and final cell sizes below that of the reference foam without particles. High contents of aerogel particles (3 wt%) led to foams with a coarser cellular structure and larger cell sizes due to an increased number of degeneration events. However, the influence of the starting isocyanate-aerogel component on the cellular structure was not assessed.

Rheology has proven to be a useful method to gain insight into the dispersion quality in composites [14–17]. For instance, the formation of a network of interconnected particles can be detected from the volume fraction dependency of the low frequency storage modulus. By using a power-law relationship it is possible to obtain the percolation threshold of the composite and assess the dispersion state [16]. Both the initial viscosity of the components and the dispersion state influence the dynamic generation of the cellular structure [18,19]. It is well known that a faster polymerisation and modulus build-up can be an effective way of producing foams with smaller cell sizes while preventing degeneration [20,21]. Yet, there are few reports analysing the impact of the initial rheological behaviour and the viscoelastic transformations on the final polymer matrix organisation of RPU foams.

In the present work, the effect of silica aerogel particles on the rheological behaviour of the isocyanate component used to produce the RPU composite foams is evaluated. In addition, the effect of the aerogel particles on the rheological changes experienced during the reaction and curing of the foams is studied *in situ* using oscillatory shear rheology. Moreover, the present paper offers insight into how the rheological properties of the raw materials and reactive mixture modify the final polymer matrix distribution.

2. Materials and methods

2.1. Raw materials of the composite RPU foams

The polyol component was a blend of two high functionality polyether polyols, Alcupol R4520 (functionality of 4.5, OH value of 455 mg·KOH g^{-1}, viscosity: 5250 mPa s at 25 °C) and Alcupol R3810 cross-linker (functionality of 3, OH value of 380 mg·KOH g^{-}, viscosity 350 mPa s at 25 °C), both from Repsol S.A. The isocyanate was a polymeric diphenylmethane diisocyanate (pMDI), IsoPMDI 92140 (31.5% NCO, density 1.23 g cm^{-3}, viscosity 170–250 mPa s at 25 °C) supplied by BASF. Polycat 8 (N,N-dimethyl cyclohexylamine) from Evonik was employed as a catalyst; it is a tertiary amine used primarily to promote the urethane (polyol-isocyanate) reaction. TEGOSTAB® B8522 (a non-hydrolysable polyether-polydimethylsiloxane–stabilizer) from Evonik was used as a surfactant to decrease the surface tension of the polyol and obtain superior cellular structures. Distilled water was employed as blowing agent.

Silica aerogel particles were provided in powder form by Cabot (Enova® Aerogel IC3100). According to the technical data, the particles have a density close to 0.15 g cm^{-3}, sizes ranging from 2 to 40 μm and an average pore diameter of 20 nm. In addition, the surface of the silica particles had been modified to give the powder a strong hydrophobic character [6]. The surface groups of the Silica Aerogel powder were previously studied by FTIR Spectroscopy which revealed the absence of Si-OH groups on the surface. It also permitted identifying the hydrophonic surface treatment which were Si-CH_3 bonds [6]. In other works the hydrophobicity of the powder was verified by investigating the contact angle of the Enova® Aerogel IC3100 powder with water using the sessile drop method [22]. The method indicated that the contact angle was high and close to 145°..

2.2. Preparation of the aerogel dispersions

The aerogel powder was dispersed in the isocyanate component with an overhead stirrer (EUROSTAR 60 control from IKA), equipped with a 50 mm diameter Vollrath™ Lenart-disc stirrer. Particle dispersions were performed at low shear stress values at 250 rpm for 5 min. Six weight concentrations were considered in this study: 0.5, 1.0, 2.0, 2.5, 3.0 and 3.5 wt% aerogel particles. To prepare the dispersion, the particles were added to 13 g of isocyanate.

2.3. Preparation of RPU foams

Four different RPU foams were prepared while maintaining a constant isocyanate index. The formulations are presented in Table 1. While the polyol, surfactant, catalyst, and blowing agent contents were kept constant, the concentration of fillers was increased resulting in four foams with different aerogel filler content (0 wt%, 0.5 wt%, 1 wt%, 3 wt %) dispersed in the isocyanate.

The blend of the polyols with the different components was prepared with an overhead stirrer (EUROSTAR 60 control from IKA), equipped with a 50 mm diameter Vollrath™ Lenart-disc stirrer. First, the polyol was mixed with the additives (catalyst, surfactant and blowing agent) at 250 rpm for 2 min. Secondly, the dispersion of the aerogel powder in the isocyanate component was carried out as described above (Section 2.2). Finally, to promote foam formation, a mixture of 50 g of isocyanate and polyol components was produced at 1200 rpm for 10 s. These foams were left to cure at room temperature for one week. After this period, the foams were cut, and the final density was measured.

2.4. Particle size characterisation

Particles were characterized using two complementary techniques. The morphology of the particles was explored using high-resolution micrographs obtained with Scanning Electron Microscopy (SEM) model: QUANTA 200 FEG, whereas the average size and size distribution of the commercial aerogel powder was determined using laser diffraction, Malvern Mastersizer 3000 E (Malvern Instruments Ltd.).

2.5. Density determination

Foam densities were measured as described by ASTM D1622/D1622M-14 [23]. The density (ρ) was measured on three different samples for each foam using the geometric volume which was obtained from cylinders of 3 cm height and 3 cm of diameter. The relative density (ρ_r), which equals the volume fraction of solid in the foam, was obtained as the ratio between the foam geometric density and the solid material density (1160 kg m^{-3}).

2.6. Rheology of isocyanate-aerogel dispersions

The rheological behaviour of the aerogel dispersions used to produce the composite foams was studied with a strain-controlled ARES-G2 rotational rheometer (TA Instruments). Two different geometries were used depending on the particle loading of the dispersion. For low particle contents (below 2 wt%) a double-wall concentric cylinder setup was used. For particle contents above or equal to 2 wt% a parallel plate geometry (40 mm diameter) was employed with a gap of 1 mm. The use of these two different geometries allows to measure materials with viscosities of several orders of magnitude difference. The temperature was controlled with an Advanced Peltier System (APS) and maintained at 25 °C.

For every measurement, a freshly prepared aerogel dispersion (Section 2.2) was produced. In addition, to ensure reproducible initial conditions, a preshear protocol was applied which consisted of shearing the sample at 5 s^{-1} during 300 s to break the initial particle network. Subsequently, the sample was left at rest for 500 s. The conditioning

Table 1
Formulations and aerogel concentration for the RPU composite foams.

Sample	Isocyanate Index	R4520 (ppw)	R3810 (ppw)	Surfactant (ppw)	Catalyst (ppw)	Water (ppw)	Aerogel (wt.%)
Reference	110	90	10	1	0.4	4	0.0
0.5% A	110	90	10	1	0.4	4	0.5
1.0% A	110	90	10	1	0.4	4	1.0
3.0% A	110	90	10	1	0.4	4	3.0

protocol was followed by a dynamic strain sweep measurement, which permits to assess the linear viscoelastic region of the sample. Data were collected stepwise from 0.01 up to 100 % strain with 5 points per decade at an oscillation frequency of 10 rad s^{-1}. After obtaining the linearity limits, a new sample was loaded and the preshear protocol was applied. Then, dynamic frequency sweep experiments were performed in the linear viscoelastic region using frequencies from 100 to 0.1 rad s^{-1} with 5 points per decade.

2.7. Rheology during foaming

The evolution of the rheological properties during foaming of the raw materials was followed using a stress-controlled AR-G2 rotational rheometer (TA Instruments). Due to the large volume expansion of the mixture during the reaction, a flooded parallel plate geometry was employed as suggested by Mora et al.[24]. The setup consisted of a 25 mm stainless steel plate as upper geometry, and a 55 mm diameter stainless steel cup as bottom geometry. The cup was inserted in a Peltier Concentric Cylinder which allowed accurate control of the sample temperature, fixed to 25 °C.

A sample volume of 6.25 mL was loaded into the rheometer cup immediately after mixing the isocyanate with the polyol component. Then, the rheometer head was quickly lowered to a gap of 2.5 mm between the plate and the bottom of the cup, after which the experiment was started. Since the sample starts reacting soon after mixing, the time period between finalizing the mixing and starting the experiment was kept as short as possible, of the order of 1.5 min.

Oscillatory time sweeps at a frequency of 1 rad s^{-1} were performed under controlled strain conditions for 1 h to characterise the rheological changes of the composite foam. To accommodate the large modulus build-up during curing, the strain was stepwise reduced during the experiments to remain below the linear strain limit and within the torque range of the device. A summary of the experimental conditions is given in Table 2. Each material was analysed in triplicate to check reproducibility. Due to foam expansion, both shear and elongational flow was present during the oscillatory experiment in the plate/plate rheometer. Hence, the obtained material properties are only apparent ones [24,25]. Yet, the comparison is still possible since all foams achieve similar expansion ratios.

2.8. X-ray tomography

The X-ray Tomography set-up used in this work is shown in Fig. 1. It consists of a microfocus X-ray source (Hamamatsu) with a maximum output power of 20 W (spot size: 5 μm, voltage: 20–100 kV, current: 0–200 μA). Emitted X-rays form a cone beam of 39°, allowing up to 20 times magnification. The transmitted X-ray intensity is collected with a high sensitivity flat panel detector connected to a frame grabber (Dalsa-Coreco), which records the projection images. The detector is composed of a matrix of 2240 × 2344 $pixels^2$, each with a size of 50 μm. Samples

Table 2
Applied strain and run times for the rheology experiments.

Time (s)	Step 1		Step 2		Step 3	
	γ_1 %	t_1 (s)	γ_2 %	t_2 (s)	γ_3 %	t_3 (s)
3600	0.5	1200	0.05	1200	0.01	1200

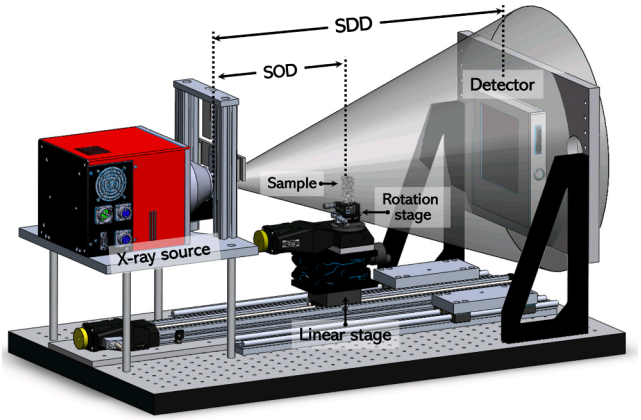

Fig. 1. 3D rendering of the laboratory X-ray tomography set-up.

were mounted on top of a rotation stage (DT-65 N from PI Micos) located between the source and detector (SDD: 581 mm). The rotation stage is positioned on top of a linear stage which permits movement between the source and detector (SOD) while modifying the magnification factor. SOD was set to 29.05 mm, yielding an effective pixel size of 2.5 μm. The scanned samples were cylinders of approximately 7 mm^2 of base and 4 mm in height. Tube voltage, current, rotation step and exposure time were set to 50 kV, 170 μA, 0.3° and 1 s respectively. Each projection was the average of three consecutive radiographies for noise reduction.

The tomography reconstructions were carried out using the Octopus package, which allowed obtaining cross-section images of the scanned volumes [26]. In the reconstructed images the fraction of mass in the struts, f_s, and struts thickness was measured using a previously reported image analysis methodology [27]. In this method, solid elements with thickness above the pixel size were binarised. Since the effective pixel size was larger than the thickness of cell walls, these were later retrieved using the Distance Transform Watershed (3D) algorithm implemented in the MorphoLibJ library (Fiji/ImageJ) [28]. Yet, with this procedure, the real walls were not retrieved as the Watershed generated walls had 2-pixel (*i.e.,* 5 μm) thickness. Nonetheless, walls were created in the right number and position, permitting to isolate neighbour cells. Afterwards, Local Thickness algorithm (Fiji/ImageJ) was applied to obtain the thickness distribution of the composite RPU-aerogel matrix [27,29]. After this step, the thickness histogram was calculated. The histogram was deconvoluted into two independent distributions depicting cell walls and struts. The deconvolution was achieved using asymmetric Log-Normal functions and from the area under each function, it was possible to obtain the tomographic value of $f_s^{\mu CT}$ using eq. (1) [27].

$$f_s^{\mu CT} = \frac{A_{st}}{A_{st} + A_w} \tag{1}$$

In eq. (1) A_{st} stands for the area under the struts, while A_w represents the area under the watershed walls distribution. To obtain the real f_s, a correction factor was applied (eq. (2)). The correction was grounded on the different relative densities obtained from the tomographic volumes, $\rho_r^{\mu CT}$, and in the foam samples, ρ_r^{Real} (see Table 3).

Table 3
Density, relative density, and cell size of the PU-aerogel composite foams.

Sample	Density (kg m^{-3})	Relative Density	Cell size (μm)
Reference	38.1 ± 0.5	0.033	412.5 ± 122.7
0.5% A	40.3 ± 0.1	0.035	309.6 ± 180.0
1.0% A	39.8 ± 0.8	0.034	290.7 ± 168.3
3.0% A	38.2 ± 0.4	0.033	454.7 ± 234.1

$$f_s = f_s^{\mu CT}\frac{\rho_r^{\mu CT}}{\rho_r^{Real}} \quad (2)$$

Struts thickness was calculated as the weighted average of the struts thickness function. In contrast, wall thickness (eq. (3)) δ was estimated using a theoretical approximation relating the thickness with the relative density of the foam, ρ_r, average cell size, Φ, the fraction of mass in the struts, f_s, and cell shape factor, C_n [30,31].

$$\Phi(1-f_s)\rho_r = C_n\delta \quad (3)$$

In eq. (3) C_n depends on the cell shape and number of faces, n. As cells in RPU foams often take the shape of pentagonal dodecahedrons the value of C_n is 3.46 [30].

3. Results and discussion

3.1. Aerogel powder characterisation

The particle size distribution was examined using Laser diffraction (Fig. 2 (a)). The technique revealed that the commercial aerogel particles had sizes ranging from 5 to 25 μm. The largest size detected was close to 25 μm, a considerably smaller value than the maximum size reported by the supplier (Section 2.1). From the volume fraction distribution of particle sizes, the volume mean diameter (eq. (4)) was calculated using the volume frequency, f_i, of particles in each size range, D_i.

$$D[4,3] = \frac{\sum D_i^4 f_i}{\sum D_i^3 f_i} \quad (4)$$

The resulting volume mean diameter was 10.9 μm, which agrees with the mean of the distribution in Fig. 2 (a). In addition, SEM micrographs (Fig. 2 (b)) also revealed irregular particles of quasi-spherical shape with a size close to 10 μm.

3.2. Composite foams density

Table 3 summarises the densities and relative densities of the large foams prepared in a 1 L disposable cup following the procedure in Section 2.3. As reported in previous work [32], density scarcely changed with the inclusion of aerogel particles. The sample with 3.0 wt% of aerogel particles had the same density as the reference foam (without aerogel particles). On the contrary, foams with low aerogel content (0.5% A and 1.0% A) displayed a 5% increase in density with respect to the reference material.

In addition, representative tomographic cross-sections of the cellular structure of the composite foams are shown in Fig. 3. A progressive cell size decrease is seen with increasing aerogel concentration for composites with less than 1 wt% of aerogel particles while a larger cell size is observed for the sample with 3.0 wt% of aerogel particles. In Table 3 the average cell size, calculated as the diameter of a sphere with equivalent volume, is included [6].

3.3. Rheology of the isocyanate-aerogel dispersions

Fig. 4 displays the dependence of the complex viscosity of the isocyanate-aerogel dispersions on the applied angular frequency (ω). The pure isocyanate exhibits a characteristic Newtonian fluid behaviour with its complex viscosity ($\eta^* = 0.32$ Pa s) independent of the applied frequency. With the addition of aerogel particles, the complex viscosity starts to increase. At high frequencies and low concentrations ($\leq$1 wt%), the dispersions reveal only a slight increase in η^* and a high frequency plateau is still visible. When the particle concentration rises beyond 1 wt %, η^* increases substantially across the entire frequency range and becomes strongly non-Newtonian and highly dependent on the oscillation frequency. At the highest concentrations, η^* even becomes reversely proportional to ω (slope close to -1). Moreover, at low frequencies, the complex viscosity of the dispersion with only 3 wt% of aerogel is nearly 5 orders of magnitude higher than the original isocyanate.

The viscoelastic nature of the dispersions is further explored by considering the storage (G') and loss (G'') modulus variation with angular frequency (Fig. 5). The pure isocyanate exhibits the expected slope of 1 for G'' versus ω and approaches a slope of 2 for G', corresponding to Newtonian fluids. With the incorporation of aerogel, both G' and G'' increase across the entire frequency spectrum.

In the high-frequency range, the loss modulus of the dispersions (Fig. 5 (b) still shows viscous behaviour, characteristic of the isocyanate matrix, since curves of G'' remain parallel to the pure isocyanate. However, with increasing aerogel content (greater than 2.5 wt%.) G'' becomes more frequency independent with a small minimum at intermediate frequencies [33].

The impact of the aerogel addition is more severe on the storage modulus. G' undergoes a steep increase with increasing particle concentration while the slope of the curve decreases drastically even at low concentrations of aerogel (75% reduction in the slope with the addition of only 0.5 wt%). As particle concentration increases, G' completely exceeds G'' indicating a liquid-to-solid transition at approximately 2.5

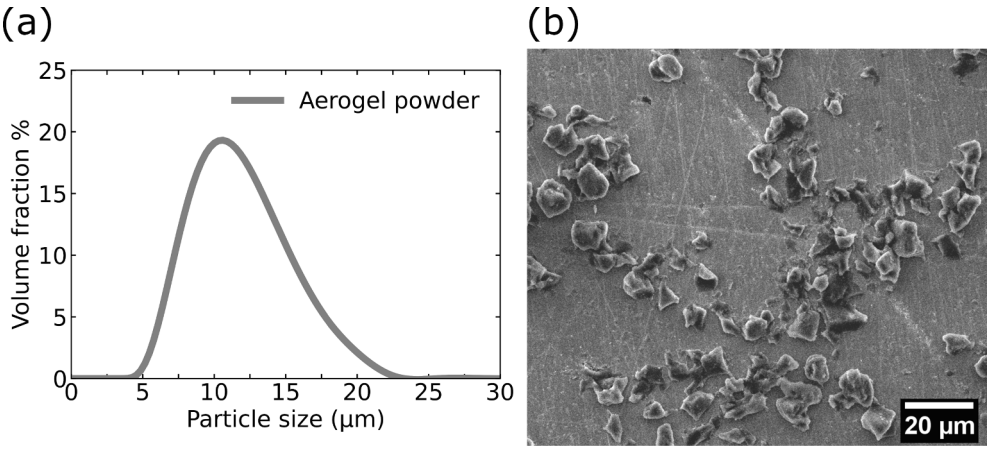

Fig. 2. (a) Enova aerogel powder size distribution measured with Laser diffraction, (b) SEM micrographs of the aerogel powder dispersed in ethanol.

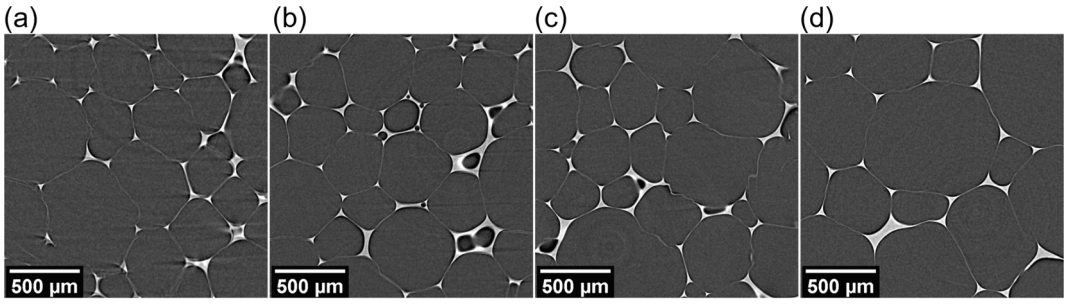

Fig. 3. X-ray tomography reconstructed slices of (a) Reference, (b) 0.5% A, (c) 1.0% A and (d) 3.0% A.

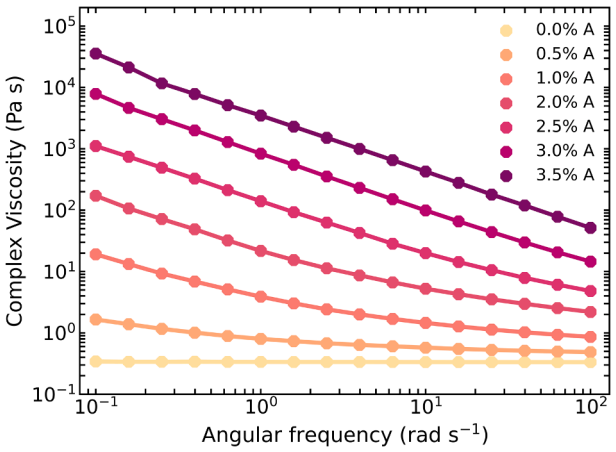

Fig. 4. Complex viscosity as a function of the angular frequency of the isocyanate-aerogel dispersions with different particle loadings.

wt%. At this concentration, G' starts to display a constant value over the entire frequency range as the slope approaches 0. The typical behaviour of G' and G'' and the corresponding decrease in η^* as a function of frequency at high aerogel concentrations is characteristic of strong gel materials [33,34], suggesting that the particle–particle interactions dominate over the polymer-particle interactions and a percolating network of touching particles is created providing the dispersions with increased elasticity [15,35].

Percolation models indicate that above a certain particle content, the low frequency storage modulus is highly dependent on the volume fraction [15,16]. This dependence of the elastic properties on the volume fraction can be expressed in the form of a power-law relationship.

$$G' \propto (\Phi - \Phi_P)^v \quad (5)$$

In eq. (5), G' is the storage modulus at low frequencies, Φ stands for the volume fraction of particles, Φ_p is the percolation threshold and v is the power-law exponent. Hence, by fitting the experimental storage modulus values at the lowest accessible frequency in Fig. 5 (a), the percolation threshold can be calculated. The volume fraction of particles is calculated assuming an aerogel density of 0.15 g cm^{-3} (Section 2.1). Yet, as a reliable fit to eq. (5) cannot always be obtained, it is assumed that, for volume fractions above the percolation threshold, the storage modulus follows a linear fit and the intersection with the x-axis yields the value of Φ_p (Fig. 6) [13,16]. Using the last three data points in in Fig. 6, a percolation threshold of 20.2 vol% is obtained, which corresponds to 2.6 wt% of aerogel, in agreement with the volume fraction at which the dispersion attains solid-like behaviour (Fig. 5).

3.4. Rheology during the composite foam development

The characterised dispersions were used to prepare the composite foams (Table 1) and their curing process was studied according to the experimental procedure detailed in Section 2.7. The evolution of the dynamic moduli and damping factor, tan δ, were monitored for 1 h (Fig. 7).

The build-up of the viscoelastic moduli is severely impacted by the addition of aerogel particles. Foams prepared with low contents of aerogel (≤1 wt%) begin the foaming process in a viscous fluid state ($G'' > G'$ and tan $\delta > 1$), with the liquid like behaviour of the individual components dominating the behaviour of the mixture. For these samples, gelling (G' and G'' crossover shown in the insets of Fig. 7) takes

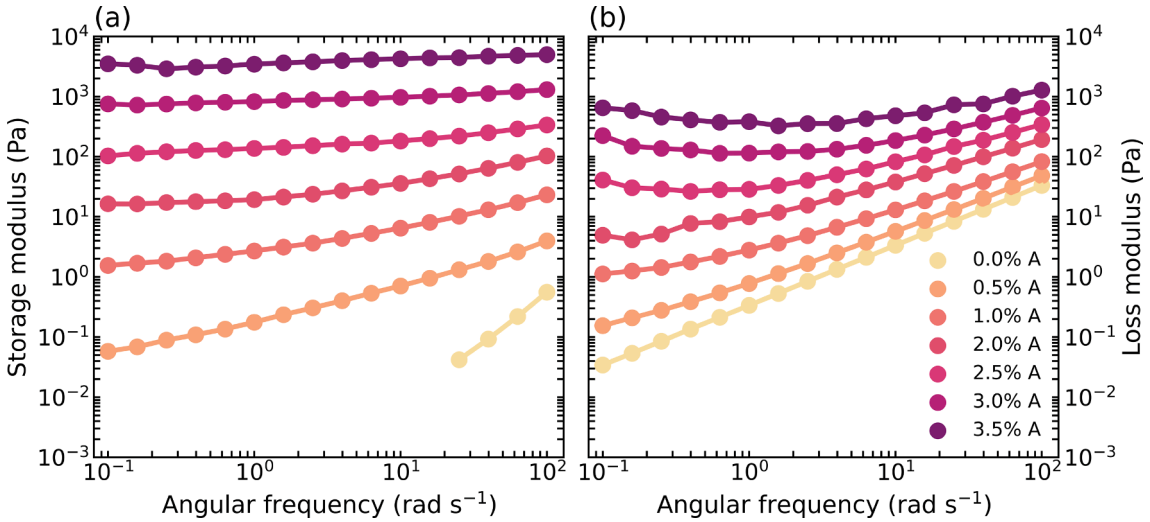

Fig. 5. Frequency sweeps of the isocyanate-aerogel dispersions with different aerogel concentrations. Storage (a) and loss modulus (b) versus angular frequency.

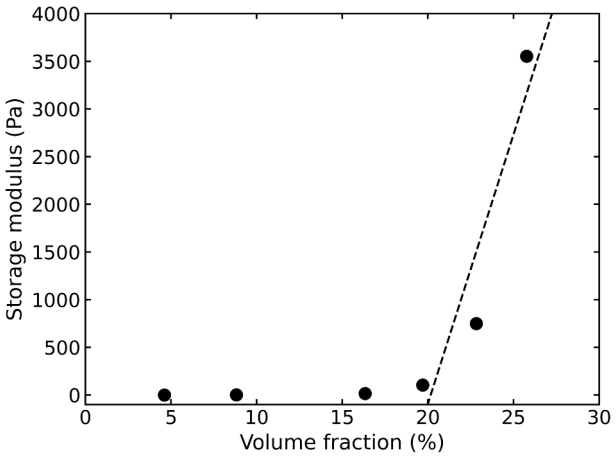

Fig. 6. Variation of the storage modulus at 0.1 rad s^{-1} with the volume fraction of aerogel particles in the dispersion.

place approximately 2.3 min after mixing (Table 4). The composite with 3 wt% of aerogel particles (Fig. 4 (d)) already displays gel-like properties ($G' > G''$) at the start of the measurement since the dispersion used to produce this material is in a percolated state where particle interactions dominate (Section 3.3). Hence, despite the incorporation of a viscous polyol phase to prepare the composite, the initial rheological response of the mixture is dominated by the gel-like particle dispersion.

Upon gelation, all foams exhibit a solid-like response ($G' > G''$) accompanied by a slow increase of the moduli. During this period, the loss modulus remains nearly constant, while the storage component slowly increases [36]. The duration of this stage depends on the content of particles in the composite. Overall, the higher the aerogel content the longer this intermediate plateau. Previous studies have linked this plateau at early curing times to the behaviour of liquid foams, whose moduli remain nearly constant at high porosities [24,37].

The second transition of major importance can be identified by the peak in the damping factor which represents *vitrification*. While the matrix vitrifies, both moduli undergo an increase of practically three orders of magnitude. At vitrification, molecular mobility is restricted since chemical reactions halt and become diffusion controlled [38]. While gelling times are not significantly affected by the presence of low concentrations of aerogel, vitrification is delayed by approximately 4.5 min with every extra addition of 1 wt% of aerogel to the composite (Table 4). This delay is a consequence of the drastic increase in the isocyanate viscosity associated with the aerogel incorporation (Fig. 4). High volume fractions of particles dispersed in isocyanate lower the mobility of the [NCO] reacting groups which slows down the urethane reaction between polyol and isocyanate [39].

As curing progresses to the last stages, the increase of the moduli as a function of time levels off. Both moduli reach a plateau, and the material achieves its final properties. The time required to reach the final plateau also depends on the content of particles. Reference and 0.5% A samples reach the final moduli practically at the same time, *ca.* after 40 min. On the contrary, 1.0 % A and 3.0 % A are retarded by 10 and more than 20 min, respectively. Moreover, foam 3.0 % A did not even reach the final cure moduli during the 1 h measurement time.

In Fig. 8, the complex viscosity evolution as a function of the reaction time of the four composites is shown. At early foaming times, a difference of more than one order of magnitude is detected between the low

Table 4
Characteristic times of the polymerisation process of RPU-aerogel foams.

Samples	Gel Time (min)	Vitrification time (min)
Reference	2.32 ± 0.04	16.4 ± 0.5
0.5% A	2.35 ± 0.02	17.7 ± 0.7
1.0% A	2.34 ± 0.07	20.9 ± 0.6
3.0% A	/	31.9 ± 1.7

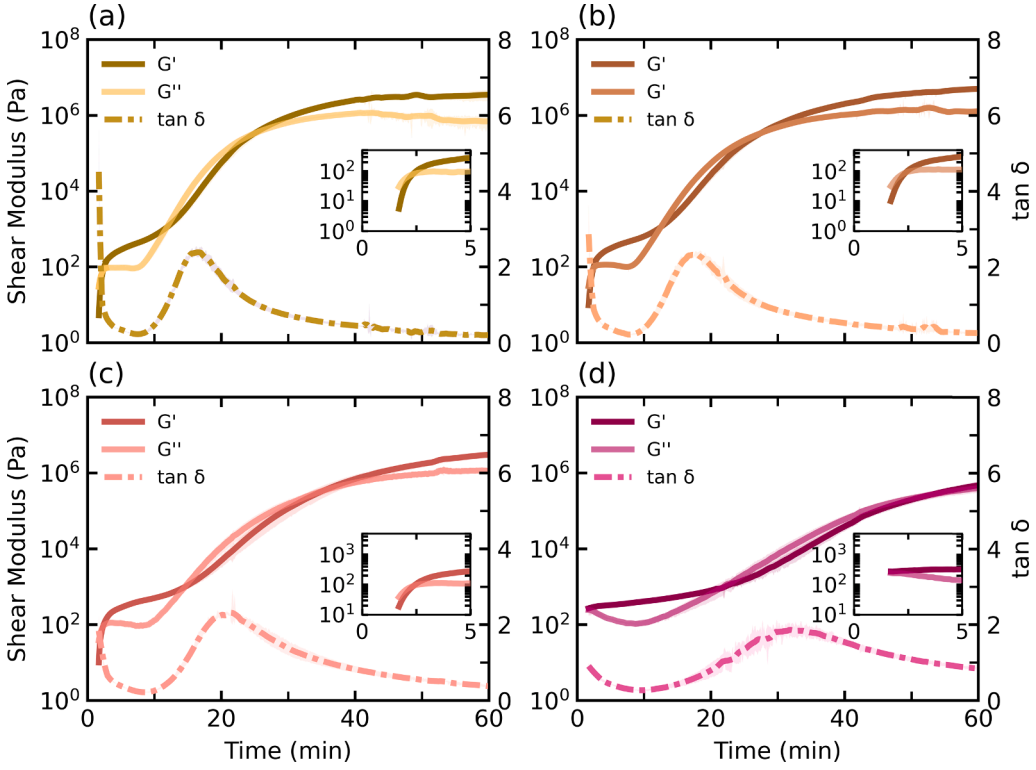

Fig. 7. Shear moduli build-up profiles at 1 rad s^{-1} for (a) Reference (0 wt% aerogel), (b) 0.5% A (0.5 wt% aerogel), (c) 1.0% A (1 wt% aerogel), (d) 3.0% A (3 wt % aerogel).

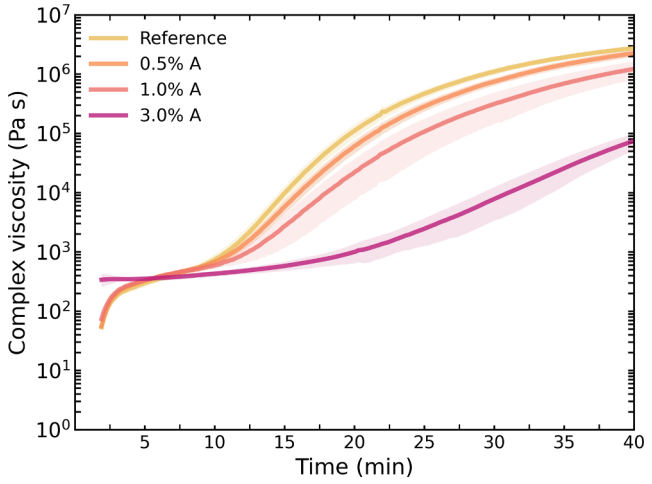

Fig. 8. Complex viscosity evolution at 1 rad/s during cure obtained from oscillatory time sweeps.

(≤1 wt%) and high aerogel content (3 wt%) composites. After the first five minutes of reaction, the complex viscosities of all foams with aerogel contents below 1 wt% start to increase gradually until reaching the onset of vitrification. At this stage the increase slows down until stabilisation is achieved. On the other hand, sample 3 % A displays a constant viscosity during the initial 20 min of reaction. After this point the viscosity gradually increases. At equal reaction times, the complex viscosity value reached by each foam decreases with increasing aerogel content.

3.5. Solid matrix characterisation

The foams prepared with 50 g of material (Section 2.3) were investigated using X-ray tomography (Section 2.8). Fig. 9 shows the thickness distribution of the polymer matrix. The wall distribution, obtained after performing Watershed segmentation, is centred at 5 μm. These walls are clearly thicker than real cell walls in RPU foams which normally have thicknesses close to 1 μm [12,40]. In contrast, the struts distribution is an accurate representation of the real struts in the foam. From Fig. 9, it is seen that the thickness of the struts increases with the incorporation of aerogel particles. Reference and 0.5 % A (Fig. 9 (a) and (b)) show very similar struts distribution of analogous maximum thickness, 57.7 μm and 54.3 μm respectively, whereas samples 1.0 % A and, in particular, 3.0 % A have a thicker matrix with a maximum thickness of 61.3 μm and 82.3 μm, respectively. The thickening of the struts with the addition of aerogel particles is also confirmed by the average strut thickness (Table 5).

The fraction of mass in the struts also changes remarkably with the aerogel content in the composite foams (Table 5). At low contents of aerogel, the struts' relative volume fraction grows with increasing thickness of these elements, thus the higher the particle content, the higher f_s. However, for the material produced with a percolated dispersion (3 wt% of aerogel) the fraction of mass in the struts decreases despite showing thicker struts than the other foams.

In addition, average wall thickness was determined through a theoretical calculation based on eq. (3). The equation predicts a steady decrease in the cell wall thickness at low contents of aerogel particles. These foams show remarkably thin cell walls, below 1 μm, because of their small cell size and high porosity. In contrast, the cell walls thicken for a particle content of 3 wt%. This thickening is related to the detected decrease in the fraction of material in the struts.

4. Discussion

Polyurethane foams typically reveal polymer phase distributions with thin cell walls and the majority of the material is located in large

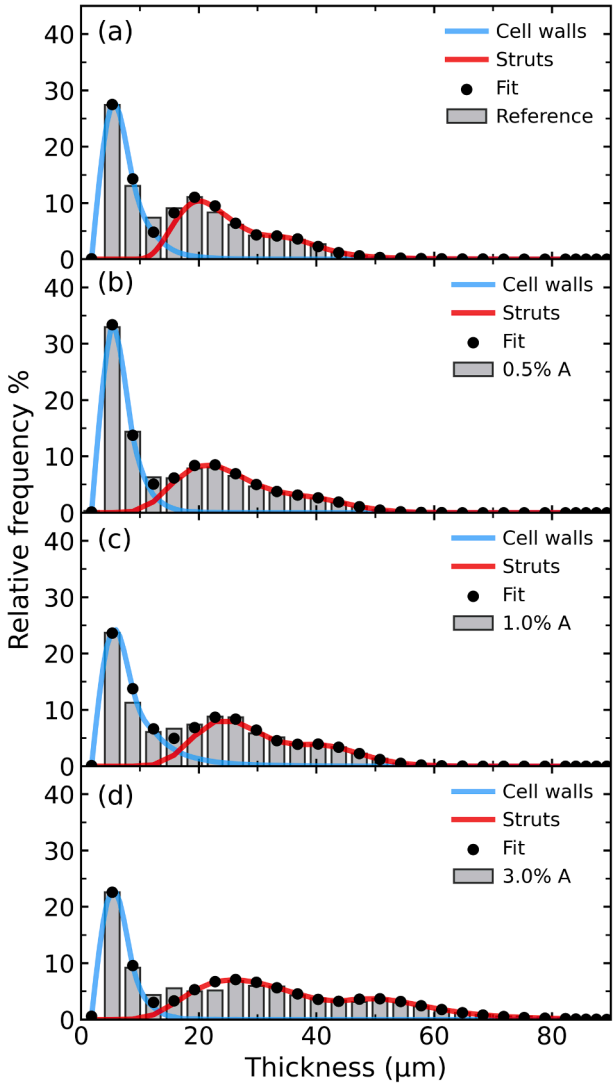

Fig. 9. (a) Reference, (b) 0.5% A, (c) 1.0% A and (d) 3.0% A matrix thickness distributions. In blue, cell walls distributions and red, struts distributions were obtained from a combination of two Log-Normal functions.

Table 5
Fraction of mass in the struts and thickness of the struts and walls (eq. (3)).

Samples	Struts thickness (μm)	Walls thickness (μm)	f_s
Reference	37.46	1.02	0.74
0.5% A	40.56	0.79	0.75
1.0% A	43.69	0.40	0.86
3.0% A	56.42	0.91	0.79

struts ($f_s \approx 0.7$) [30,40]. The high fraction of mass in the struts is due to a foaming process prone to drainage from the cell walls to the struts when the mixture is in a fluid state. Factors such as the viscosity of the reactive mixture, the amount of gas being generated, and the speed of polymerisation drastically modify the intensity of degeneration mechanisms and the flow of material from the walls to the struts [41–43].

For the composite foams in this study, the thickness of the struts was observed to increase linearly with the addition of aerogel whereas the fraction of polymer in the struts changed non-linearly with the content of particles (Section 3.5). In previous work, the destabilizing effect of aerogel particles on the structure during foaming was revealed [6]. The micrometric particles trigger a large number of degeneration mechanisms, especially coalescence and broken cell walls, which cause cell size

to increase long after foam expansion has stopped. Upon coalescence, two growing cells merge as a result of cell wall rupture. It was found that aerogel particles cause degeneration by two mechanisms: local thinning due to drainage and rupture of the walls by particles larger than the thickness of the cell walls [6,44]. The drainage rate is known to be inversely proportional to the viscosity. Hence, at high viscosities, the flow of the material to the struts is retarded and the walls can remain longer at thickness above the critical rupture value [44].

Fig. 6 shows that mixtures with low aerogel contents ($\leq$1 wt%) present a fluidlike viscous response at early foaming stages, similar to that of the starting isocyanate-aerogel dispersions (Fig. 5). According to the literature, it is expected that the low viscosity mixture undergoes severe drainage to the struts upon impingement of the cells [43,44]. This intense flow drags most of the aerogel particles to the struts (Fig. 10), explaining the detected thickening of the struts in the final foams (Table 5). Moreover, drainage involves local thinning of the walls which explains the high number of cell wall ruptures detected at short foaming times (<5 min) as reported in previous work [6]. Based on SEM images, aerogel particles are also found to detach from the solid matrix and locate inside the cells (Fig. 10 (a)). Potentially, a fraction of the large particles or aggregates are forced out of the walls. Drainage and coalescence proceed while the elastic component of the modulus is low ($G' \lesssim 10^3$ Pa). Consequently, upon solidification of the matrix (caused by the onset of vitrification, t $\approx$ 10 min) foams reveal a structure with a higher fraction of polymer in the struts and lower cell wall thickness than the unfilled reference foam (Table 5).

However, the composite with high content of aerogel particles (3 wt %) presented a completely different rheological development and final structure. At high aerogel concentrations, a percolating network of particles was created, and the isocyanate dispersion showed the viscoelastic fingerprint of a strong gel (Fig. 5). After stirring the components, the reactive mixture inherited the gel-like behaviour of the isocyanate-aerogel dispersion (Fig. 7). Hence, foaming began with the mixture in a highly viscous gel-like state (Section 3.4) responsible for the slow foam expansion observed in previous work [6]. Moreover, the high viscosity of the mixture also slowed down the drainage of reactive material and aerogel to the struts. Despite the reduction in drainage, coalescence in foam 3 % A was not inhibited and, in fact, it was detected throughout the whole foaming process (11 min) [6]. On the one hand, the main mechanism responsible for coalescence is the disrupting effect of a high volume fraction (more than 20 vol%) of micrometric particles in the foam matrix. When the particles are located in the stiffening walls, the critical wall thickness is reduced triggering wall ruptures and a partially open cell structure in the final foams, which was not observed in the other composites [6]. Upon coalescence, the polymer mass located in the missing cell walls is redistributed between the struts and walls of the new cell, thickening the overall matrix. On the other hand, the enduring coalescence corresponds to the slower modulus build-up and delayed matrix vitrification, meaning that full hardening of the matrix takes longer to be achieved for the foam 3% A (Table 4). Therefore, the aforementioned phenomena are responsible for decreasing the fraction of polymer in the struts (Table 5). To summarise the previous ideas, drainage to the struts is slowed down by the high viscosity of the initial mixture, whereas coalescence, caused by aggregates, leads to larger cells with a thicker surrounding matrix which undergoes slow drainage and results in thicker cell walls than the composites with low aerogel content. Yet, while foam 3% A was prepared with a percolated dispersion of touching particles it was not possible to confirm by X-ray tomography whether the particles were also intercconneted within the solid matrix of the foam. However, SEM micrographs of the structure of the composite foams (Fig. 10) revealed the existence of a high density of particles in the struts of the cells. The particles can be detected both in the areas of the struts exposed by the cross-sectional cut and also embedded in the non-exposed struts. These particles show up as rugosities in the otherwise smooth struts. In addition, examination of the SEM micrographs confirmed the absence of aerogel particles in the cell walls. This is most likely due to the reduced thickness of the walls (Table 5) in which the aerogel particles do not fit due to their large size (~10 μm).

5. Conclusions

The present study reveals that foams with low contents of aerogel particles ($\leq$1 wt%) undergo an increase in the fraction of mass in the struts with increasing concentration of particles. This increase is accompanied by a thickening of the struts as the result of the drainage of both polymer and aerogel particles from the walls to the struts. This intense drainage is a consequence of the low viscosity of the isocyanate-aerogel dispersions used to produce the RPU composite foams. At low concentrations of aerogel, the dispersions exhibit a fluid-like response and upon reaction with the polyol, the reactive mixtures have low viscosities until gelation is reached. Conversely, both the rheological behaviour and polymer matrix distribution change drastically at a particle content of 3 wt%. The analysis of the low frequency values of the storage modulus of the starting isocyanate-aerogel component reveals that the percolation threshold weight fraction is at 2.6 wt%. Hence, in the dispersion with 3 wt% of aerogel, the particles form an interconnected structure that restrains the motion of the polymer chains. In addition, the isocyanate-aerogel dispersion has a high viscosity which causes the 3.0% A composite foam to start its foaming process already in a gel-like state. For that reason, the material undergoes less drainage during foaming and the final composite foam reveals a polymer matrix distribution with a lower fraction of material in the struts and thicker cell walls.

CRediT authorship contribution statement

Paula Cimavilla-Román: Conceptualization, Data curation, Investigation, Methodology, Formal analysis, Writing – original draft. **Saul Perez-Tamarit:** Data curation, Methodology, Investigation. **Anja Vananroye:** Validation, Investigation, Supervision, Methodology,

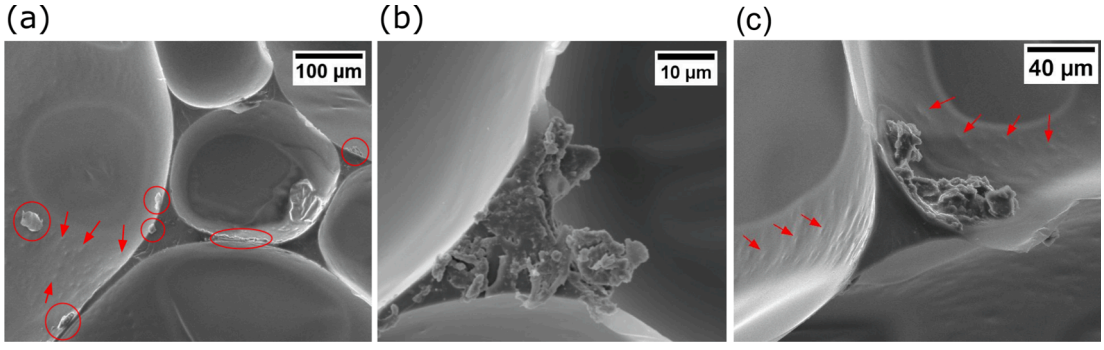

Fig. 10. SEM images of the polymer matrix revealing particles (a) detached from the matrix (foam 1% A), (b) and (c) embedded in the struts (foams 3% A). Arrows indicate particles non exposed by the cross-sectional cut but embedded in the struts and also those showing up as ruggosities.

Writing – review & editing. **Paula Moldenaers:** Validation, Supervision, Resources, Writing – review & editing. **Miguel Ángel Rodriguez-Pérez:** Conceptualization, Validation, Resources, Supervision, Project administration, Funding acquisition, Writing – review & editing.

Declaration of Competing Interest

The authors declare that they have no known competing financial interests or personal relationships that could have appeared to influence the work reported in this paper.

Acknowledgements

Financial assistance from the Junta of Castile and Leon (VA202P20) and Spanish Ministry of Science, Innovation and Universities (RTI2018-098749-B-I00 and RTI2018 - 097367-A-I00) is gratefully acknowledged. Financial support from Junta de Castilla y Leon predoctoral grant of P. Cimavilla-Román, co-financed by the European Social Fund, is also acknowledged.

Data availability statement

The raw/processed data required to reproduce these findings cannot be shared at this time as the data also forms part of an ongoing study.

References

[1] T. Sabu, K. Joseph, S.K. Malhotra, K. Goda, M.S. Sreekala, Polymer Composites, Macro- and Microcomposites, 1st ed., Wiley-VCH Verlag, 2012.
[2] L. Verdolotti, M.R. Di Caprio, M. Lavorgna, G.G. Buonocore, Polyurethane Nanocomposite Foams: Correlation Between Nanofillers, Porous Morphology, and Structural and Functional Properties, in: Polyurethane Polym. Compos. Nanocomposites, Elsevier Inc., 2017: pp. 277–310.
[3] V. Mittal, Polymer Nanocomposite Foams, First Edit, CRC Press, Abu Dhabi, 2013.
[4] H. Sanaeishoar, M. Sabbaghan, F. Mohave, Synthesis and characterization of micro-mesoporous MCM-41 using various ionic liquids as co-templates, Microporous Mesoporous Mater. 217 (2015) 219–224.
[5] K.-J. Chang, Y.-Z. Wang, K.-C. Peng, H.-S. Tsai, J.-R. Chen, C.-T. Huang, K.-S. Ho, W.-F. Lien, Preparation of silica aerogel/polyurethane composites for the application of thermal insulation, J. Polym. Res. 21 (1) (2014).
[6] P. Cimavilla-Román, S. Pérez-Tamarit, M. Santiago-Calvo, M.Á. Rodríguez-Pérez, Influence of silica aerogel particles on the foaming process and cellular structure of rigid polyurethane foams, Eur. Polym. J. 135 (2020), 109884.
[7] Y.X. Thong, X. Li, X.J. Yin, Determining the best flame retardant for rigid polyurethane foam—Tris(2-chloroisopropyl) phosphate, expandable graphite, or silica aerogel, J. Appl. Polym. Sci. 139 (2022) 51888.
[8] C. Zhao, Y. Yan, Z. Hu, L. Li, X. Fan, Preparation and characterization of granular silica aerogel/polyisocyanurate rigid foam composites, Constr. Build. Mater. 93 (2015) 309–316.
[9] A. Dourbash, C. Buratti, E. Belloni, S. Motahari, Preparation and characterization of polyurethane/silica aerogel nanocomposite materials, J. Appl. Polym. Sci. 134 (2017) 1–13.
[10] E. Hamamizadeh, H.A. Mahabadi, A. Khavanin, Investigating the Mechanical, Morphological, and Acoustic Properties of the Phenolic Aerogel/Flexible Polyurethane Foam Composite, J. Polym. Environ. 30 (6) (2022) 2483–2492.
[11] J.-H. Kim, J.-H. Ahn, J.-D. Kim, D.-H. Lee, S.-K. Kim, J.-M. Lee, Influence of Silica-Aerogel on Mechanical Characteristics of Polyurethane-Based Composites: Thermal Conductivity and Strength, Materials (Basel). 14 (2021) 1790.
[12] M. Santiago-Calvo, J. Tirado-Mediavilla, J.L. Ruiz-Herrero, M.Á. Rodríguez-Pérez, F. Villafañe, The effects of functional nanofillers on the reaction kinetics, microstructure, thermal and mechanical properties of water blown rigid polyurethane foams, Polymer (Guildf). 150 (2018) 138–149.
[13] M. Akkoyun, E. Suvaci, Effects of TiO2, ZnO, and Fe3O4 nanofillers on rheological behavior, microstructure, and reaction kinetics of rigid polyurethane foams, J. Appl. Polym. Sci. 133 (2016) 1–14.
[14] F.J. Galindo-Rosales, P. Moldenaers, J. Vermant, Assessment of the dispersion quality in polymer nanocomposites by rheological methods, Macromol. Mater. Eng. 296 (2011) 331–340.
[15] R. Van Hooghten, S. Gyssels, S. Estravis, M.A. Rodriguez-Perez, P. Moldenaers, Understanding the effect of particle surface free energy on the structural and mechanical properties of clay-laden rigid polyurethane foams, Eur. Polym. J. 60 (2014) 135–144.
[16] J. Vermant, S. Ceccia, M.K. Dolgovskij, P.L. Maffettone, C.W. Macosko, Quantifying dispersion of layered nanocomposites via melt rheology, Journal of Rheology 51 (3) (2007) 429–450.
[17] A. Ballesteros, E. Laguna-Gutierrez, P. Cimavilla-Roman, M.L. Puertas, A. Esteban-Cubillo, J. Santaren, M.A. Rodriguez-Perez, Influence of the dispersion of Nanoclays on the cellular structure of foams based on polystyrene, J. Appl. Polym. Sci. 138 (2021) 1–19.
[18] B. Merillas, F. Villafañe, M.Á. Rodríguez-Pérez, Nanoparticles Addition in PU Foams: The Dramatic Effect of Trapped-Air on Nucleation, Polym. 2021, Vol. 13, Page 2952. 13 (2021) 2952. (accessed January 12, 2022).
[19] M. Mar Bernal, S. Pardo-Alonso, E. Solórzano, M.Á. Lopez-Manchado, R. Verdejo, M.Á. Rodriguez-Perez, Effect of carbon nanofillers on flexible polyurethane foaming from a chemical and physical perspective, RSC Adv. 4 (2014) 20761.
[20] M. Santiago-Calvo, V. Blasco, C. Ruiz, R. París, F. Villafañe, M.-Á. Rodríguez-Pérez, Synthesis, characterization and physical properties of rigid polyurethane foams prepared with poly(propylene oxide) polyols containing graphene oxide, Eur. Polym. J. 97 (2017) 230–240.
[21] M. Santiago-Calvo, S. Pérez-Tamarit, P. Cimavilla-Román, V. Blasco, C. Ruiz, R. París, F. Villafañe, M.Á. Rodríguez-Pérez, X-ray radioscopy validation of a polyol functionalized with graphene oxide for producing rigid polyurethane foams with improved cellular structures, Eur. Polym. J. 118 (2019) 404–411.
[22] F. Raoufi, Z. Ranjbar, S. Rategar, E. Nowak, B. Nazari, Wettability study of super-hydrophobic silica aerogel powders, Prog. Color. Color. Coatings. 13 (2020) 75–83. (accessed June 20, 2022).
[23] ASTM D1622-08: Standard Test Method for Apparent Density of Rigid Cellular Plastics, (n.d.).
[24] E. Mora, L.D. Artavia, C.W. Macosko, Modulus development during reactive urethane foaming, J. Rheol. 35 (5) (1991) 921–940.
[25] R. Bouayad, J. Bikard, J.F. Agassant, Compressible flow in a plate/plate rheometer: Application to the experimental determination of reactive expansion's models parameters for polyurethane foam, Int. J. Mater. Form. 2 (2009) 243–260.
[26] M. Dierick, B. Masschaele, L.V. Hoorebeke, Octopus, a fast and user-friendly tomographic reconstruction package developed in LabView®, Meas. Sci. Technol. 15 (7) (2004) 1366–1370.
[27] P. Cimavilla-Román, S. Pérez-Tamarit, S. Barroso-Solares, J. Pinto, M.Á. Rodríguez-Pérez, Sub-pixel Tomographic Methods for Characterizing the Solid Architecture of Foams, Microsc. Microanal. 28 (3) (2022) 689–700.
[28] D. Legland, I. Arganda-Carreras, P. Andrey, MorphoLibJ: Integrated library and plugins for mathematical morphology with ImageJ, Bioinformatics. 32 (2016) 3532–3534.
[29] R. Dougherty, K.-H. Kunzelmann, Computing Local Thickness of 3D Structures with ImageJ, Microsc. Microanal. 13 (2007) 1678–1679.
[30] S. Pardo-Alonso, E. Sorlórzano, L. Brabant, P. Vanderniepen, M. Dierick, L. Van Hoorebeke, M.A. Rodríguez-Peréz, 3D Analysis of the progressive modification of the cellular architecture in polyurethane nanocomposite foams vía X-ray microtomography, Eur. Polym. J. 149 (2013) 999–1006.
[31] N.C. Hilyard, A. Cunningham, Low density cellular plastics, 1st Ed, Springer Science & Business Media, 2012, London, 1994.
[32] P. Cimavilla-Román, M. Santiago-Calvo, M.Á. Rodríguez-Pérez, Dynamic Mechanical Analysis during polyurethane foaming: Relationship between modulus build-up and reaction kinetics, Polym. Test. 103 (2021), 107336.
[33] C. Vallés, R.J. Young, D.J. Lomax, I.A. Kinloch, The rheological behaviour of concentrated dispersions of graphene oxide, J. Mater. Sci. 49 (18) (2014) 6311–6320.
[34] T. Varzakas, C. Tzia, Food engineering handbook: Food engineering fundamentals, Food Eng. Handb. Food Eng. Fundam. (2014) 1–569.
[35] S. Thankappan Nair, P.P. Vijayan, P. Xavier, S. Bose, S.C. George, S. Thomas, Selective localisation of multi walled carbon nanotubes in polypropylene/natural rubber blends to reduce the percolation threshold, Compos. Sci. Technol. 116 (2015) 9–17.
[36] M.-C. Jawhar, D. Blanc, P. Chaumont, P. Cassagnau, Study of the Coalescence Mechanisms During Silicone Foaming, Macromol. Mater. Eng. 299 (3) (2014) 336–343.
[37] H.M. Princen, A.D. Kiss, Rheology of Foams and Highly Concentrated Emulsions III. Static Shear Modulus, J. Japanese Soc Hortic. Sci. 65 (1996) 121–127.
[38] C. Block, B. Van Mele, P. Van Puyvelde, G. Van Assche, Time-temperature-transformation (TTT) and temperature-conversion- transformation (TxT) cure diagrams by RheoDSC: Combined rheometry and calorimetry on an epoxy-amine thermoset, React. Funct. Polym. 73 (2013) 332–339.
[39] M. Abdalla, D. Dean, P. Robinson, E. Nyairo, Cure behavior of epoxy/MWCNT nanocomposites: The effect of nanotube surface modification, Polymer (Guildf). 49 (15) (2008) 3310–3317.
[40] S. Pérez-Tamarit, E. Solórzano, A. Hilger, I. Manke, M.A. Rodríguez-Pérez, Multi-scale tomographic analysis of polymeric foams: A detailed study of the cellular structure, Eur. Polym. J. 109 (2018) 169–178.
[41] L.W. Schwartz, R.V. Roy, A mathematical model for an expanding foam, J. Colloid Interface Sci. 264 (1) (2003) 237–249.
[42] P. Ferkl, I. Krśková, J. Kosek, Evolution of mass distribution in walls of rigid polyurethane foams, Chem. Eng. Sci. 176 (2018) 50–58.
[43] S.T. et al. Lee, Polymeric Foams: Science and Technology, Taylor & Francis, Boca Raton, 2007.
[44] N.S. Ramesh, S.T. Lee, Polymeric Foams: Mechanisms and Materials, First Ed, CRC Press, Boca Raton, 2004.